DRAFT(2nd)
Procedure for extraction of difference of cross sections.

Kang, Hyekoo
Seoul National University

November 22, 2011

Abstract

The method of extracting the experimental/simulated ratio of difference of cross sections is described. Cross sections are obtained via simulations and extracted from the experimental data. Beam energy of 2.260 GeV is used and the ratios are obtained in function of scattering angle. This note describes the elastic analysis but the similar procedure would be applied to inelastic domain.

1 Prerequisites

Basic cuts for selection of elastic events are applied. Those are:

1. $0.9 \leq$ invariant mass ≤ 1.0
2. $gpart > 0$, $q[0] < 0$
3. $dc\_stat[dc[0]-1] > 0$, $stat[0] > 0$
4. $cc[0] > 0$, $cc[0] \leq cc\_part$, $dc[0] > 0$, $dc[0] \leq dc\_part$
5. $sc[0] > 0$, $sc[0] \leq sc\_part$, $ec[0] > 0$, $ec[0] \leq ec\_part$
6. $p[0] > 0.3$, $dc\_sect[dc[0]-1] == 6$, $hel\_flag > 0$

The cut 1 is for selection of elastic events(W_{proton} is about 0.93827 GeV.). And other cuts are from the group 1 and 2 at the reference [6]. Those are for: requiring at least one particle recorded for each event and the first particle(electron)'s having negative charge(2), successfully reconstructed(3) and hitting Cerenkov Counter(CC), Drift Chamber(DC), TOF scintillator(SC) and EM Calorimeter(EC)(4-5) and minimum value of reconstructed momentum, events hitting sector 6 and good helicity state(6). Because the simple simulation to be discussed in section 3 used for this analysis doesn't account for the CLAS acceptance and magnetic field, the cuts are to be chosen to

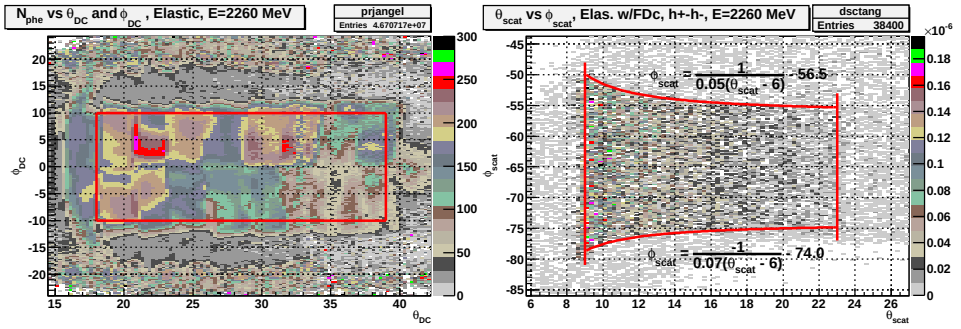

Figure 1: Left: Distribution of N_{phe} for each projected angle bin(θ_{DC},ϕ_{DC}). Right: Difference of normalized yields for each scattering angle bin(θ_{scat},ϕ_{scat}).

make the acceptance within those cuts close to unity. These cuts must be done on the vertex variables since the simulation cannot produce angular variables at the detector level. At first, fiducial area is determined via the distribution of N_{phe} which is plotted on the phase space of projected angles. The area is chosen to avoid the regions of low CC efficiency, Nphe×10 near 0. See fig. 1. The cuts can be simply chosen and those are:

- $18.0 \leq \theta_{DC} \leq 39.0$
- $-10.0 \leq \phi_{DC} \leq 10.0$

where the $\theta_{DC}(\phi_{DC})$ is the projected theta(phi) to the imaginary plane on CC[7]. Using the elastic events within the area designed by those two cuts, the yields normalized to the Faraday-cup counts per each helicity state are extracted for each bin of scattering angles, theta-phi. Then, the difference of normalized yields is obtained via the simple subtraction of those two 2-D histograms. All the target material but the hydrogens are unpolarized so the differences of yields from the material other than hydrogen are canceled, see 2-dimensional plot on the right on fig. 1. We define the cut on the vertex variable ϕ_{scat} and θ_{scat} by two straight lines and two curves. The acceptance within those boundaries is expected to be close to unity. The formulae for those boundaries are:

$$9.0 \leq \theta_{scat} \leq 23.0 \tag{1}$$

$$\phi_{scat} \leq \frac{1}{0.05(\theta_{scat} - 6)} - 56.5 \tag{2}$$

$$\phi_{scat} \geq \frac{-1}{0.07(\theta_{scat} - 6)} - 74.0 \tag{3}$$

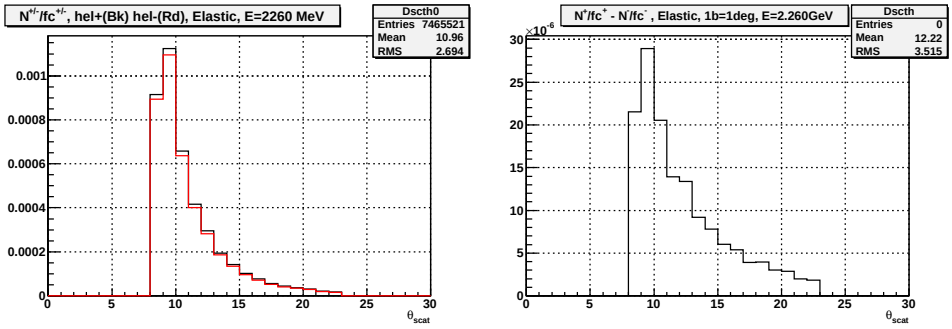

Figure 2: Faraday-cup normalized elastic yields per helicity state(Red for helicity plus and Black for minus, left) and the difference of them(right).

For experimental data, the events selected with all those cuts listed above are used to obtain the difference of elastic cross sections and the experimental/simulated ratios.

2 Experimental cross section difference

Fig. 2 shows distributions of the faraday-cup normalized yields per helicity + and -)state and their difference in terms of scattered angle. The difference of cross sections is extracted from the difference of yields. It can be written as:

$$\sigma_{diff}^{exp} = \frac{1}{N_t}\left[\frac{N^+}{N_{e^-}^+} - \frac{N^-}{N_{e^-}^-}\right] \cdot \frac{1}{\Delta\Omega} \cdot DE \tag{4}$$

where DE stands for detector efficiencies. The parameters used in eq.1 are:

- $N_t = 3N_a l_A \frac{\rho_A}{m_A}$: Number of target nulceons from hydrogen.

  $N_a = 6.02 \times 10^{23}$: Avogadro's number.

  $l_A = 1(cm) \times 0.6$: Target length and 0.6 for packing fraction.

  $\rho_A = 0.917(g/cm^3)$: Target density.

  $m_A = 18.023584(g)$: Mass of target molecule, $^{15}NH_3$.

  3 : number of hydrogen atom in the ^{15}NH$_3$ molecule.

- $N^{+/-}$: Number of scattered electrons per each helicity state(+/-).

- $N_{e^-} = (\frac{fc^{+/-} \cdot 10^{-9}}{9264}/Q_{e^-}) \cdot \frac{BPM}{f-cup}$: Number of incoming electrons.

  $fc^{+/-}$: Helicity dependent Faraday-cup counts, which is gated by live time.

$\frac{10^{-9}}{9264}$: 1/9264 [1],[2] is the conversion factor for Faraday-cup counts to be transformed into electric charge. Faraday-cup counts are recorded in nano coulomb so it's to be converted to coulomb.

$Q_{e^-} = 1.602 \times 10^{-19}(C)$: the electron's charge.

$\frac{BPM}{F-cup} = \left(\frac{F-cup}{BPM}\right)^{-1}$: inverse of Faraday cup-BPM ratio. It's 0.965919 for 2.3 GeV[5]. Faraday-cup is located at the end of the beamline and because its physical radius is not large enough, some of the beam's halo aren't collected. The size of the beam halo, i.e., the Faraday-cup loss, depends on the amount of material in the beam line and also depends on the beam energy. The BPM , situated before the target, does not suffer such loss. So the Fcup/BPM ratio recovers the number of incoming electrons. For high beam energy such as 3 GeV of EG4, it is close to 1 but is less than 1 for lower beam energy like 1.X GeV.

- $\Delta\Omega$: Solid angle for each $\langle\theta_{scat}\rangle$ bin:

  $\Delta\Omega = sin(\langle\theta_{scat}\rangle)\Delta\theta_{scat}\Delta\phi(\langle\theta_{scat}\rangle)$
  $\Delta\theta = 1^\circ \cdot \frac{\pi}{180^\circ}$
  $\Delta\phi(\langle\theta_{scat}\rangle)$ is from eq. 2 and 3:
  $\Delta\phi(\langle\theta_{scat}\rangle) = \left[\left(\frac{1}{0.05} - \frac{1}{0.07}\right)\frac{1}{\langle\theta_{scat}\rangle - 6} + 17.5\right] \cdot \frac{\pi}{180^\circ}$.

$$\begin{aligned}\Delta\Omega &= sin(\langle\theta_{scat}\rangle)\Delta\theta_{scat}\Delta\phi(\langle\theta_{scat}\rangle) \\ &= sin(\langle\theta_{scat}\rangle)\left(\frac{\pi}{180^\circ}\right)^2\left[\left(\frac{1}{0.05} - \frac{1}{0.07}\right)\frac{1}{\langle\theta_{scat}\rangle - 6} + 17.5\right] \quad (5)\end{aligned}$$

2.1 Estimation of uncertainty

Solid angle is computed at each $\langle\theta_{sc}\rangle$ bin and its corresponding $\Delta\phi_{sc}(\langle\theta_{sc}\rangle)$. The uncertainty of σ^{exp}_{diff} is to be considered. Rewrite eq. 4:

$$\sigma^{exp}_{diff} = \frac{1}{N_t}\frac{1}{\frac{10^{-9}}{9264}\frac{1}{Q_{e^-}}}\left(\frac{N^+}{fc^+\frac{1}{fbr}} - \frac{N^-}{fc^-\frac{1}{fbr}}\right)\frac{1}{\Delta\Omega}. \quad (6)$$

where fbr indicates Faraday cup-BPM ratio. Now the statistical uncertainty is:

$$\begin{aligned}\left(\Delta\sigma^{exp}_{diff}\right)^2 &= \frac{1}{N_t^2}\frac{1}{C_f^2}\left[\frac{1}{fc^{+2}}\left(fbr^2\sigma^2_{N^+} + N^{+2}\sigma^2_{fbr}\right) + \frac{1}{fc^{-2}}\left(fbr^2\sigma^2_{N^-} + N^{-2}\sigma^2_{fbr}\right)\right]\frac{1}{\Delta\Omega^2} \\ &= \frac{1}{N_t^2}\frac{1}{C_f^2}\left[fbr^2\left(\frac{\sigma^2_{N^+}}{fc^{+2}} + \frac{\sigma^2_{N^-}}{fc^{-2}}\right) + \left(\frac{N^{+2}}{fc^{+2}} + \frac{N^{-2}}{fc^{-2}}\right)\sigma^2_{fbr}\right]\frac{1}{\Delta\Omega^2}. \quad (7)\end{aligned}$$

where $C_f = \frac{10^{-9}}{9264}\frac{1}{Q_{e^-}}$, which is the conversion factor for faraday cup counts to total number of incoming electrons. $\sigma_{N^{+(-)}}$ and σ_{fbr} are the statistical errors for the helicity dependent number of events and the error of faraday cup-BPM ratios respectively.

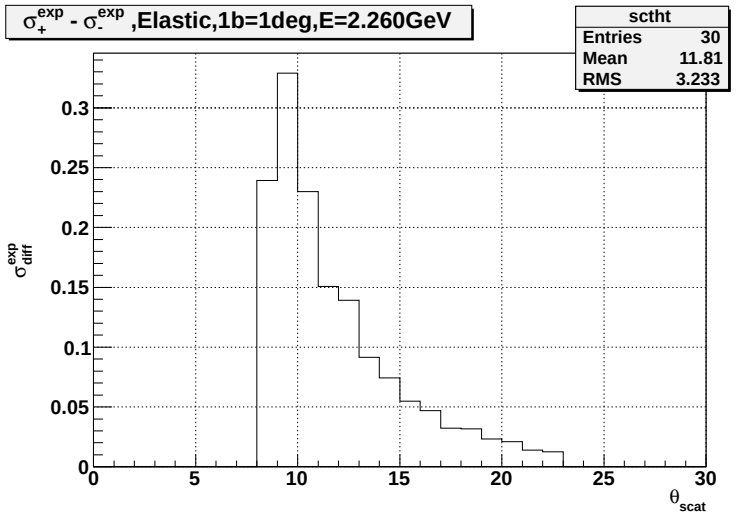

Figure 3: Difference of cross sections in terms of scattering theta.

2.2 Contaminations from ^{15}N polarizations

In case of small Q^2 value or low θ_{sc} for elastic scattering, a negative peak appears in the super-elastic region, invariant mass between 0.9 and 0.92. See, for example, fig. 4. It is suspected to be due to the small polarization of 15-nitrogen[3]. This effect is enhanced when beam energy is lowered to 1.X GeV. See figure 4. Also, see figure 5 and 6 for higher beam energies. It will be investigated later.

3 Simulated cross section difference

Simulation is based on the mce94010 program and was modified by A. Deur[4] to be used for CLAS beamline and target cell. This simulation generates the elastic events from a point-like target and does not contain any effects caused by CLAS detector such as acceptance of CLAS or its magnetic field. The consequence of not accounting for B-field and acceptance is that we have to:

- use vertex variables rather than detector variables, (discussed already.)
- we need to choose events from an area in which the acceptance is close to 1. This reduces the statistics.

The radiative effects and multiple scattering is accounted for by this simulation. To use the full EG4 statistics, GSIM, the monte carlo simulation for CLAS, should be used.

Events are generated within the rectangular area(A_s) drawn on fig. 7. The area A_c, which is equivalent to the area on the right (see red lines) in

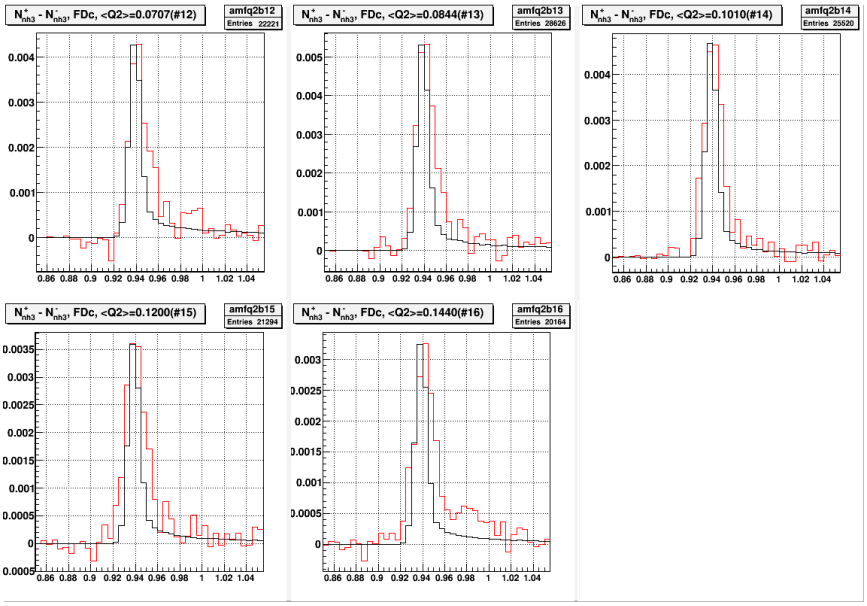

Figure 4: Difference of cross sections vs invariant mass (W) from 1.0GeV data. Red from data and Black from simulation. A small negative peak is visible between 0.9 and 0.92.

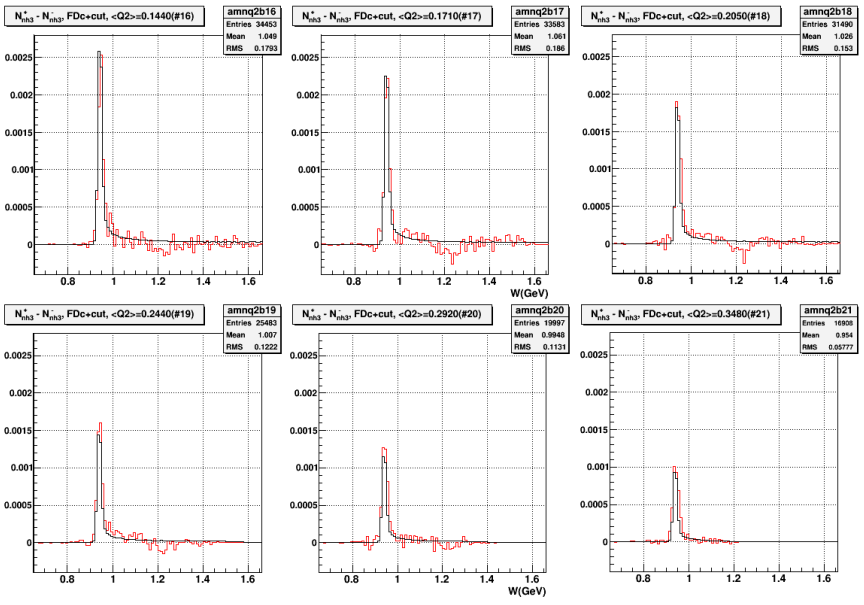

Figure 5: Difference of cross sections vs invariant mass (W) from 2.3GeV data. Red from data and Black from simulation. A small negative peak is rarely visible or disappeared between 0.9 and 0.92.

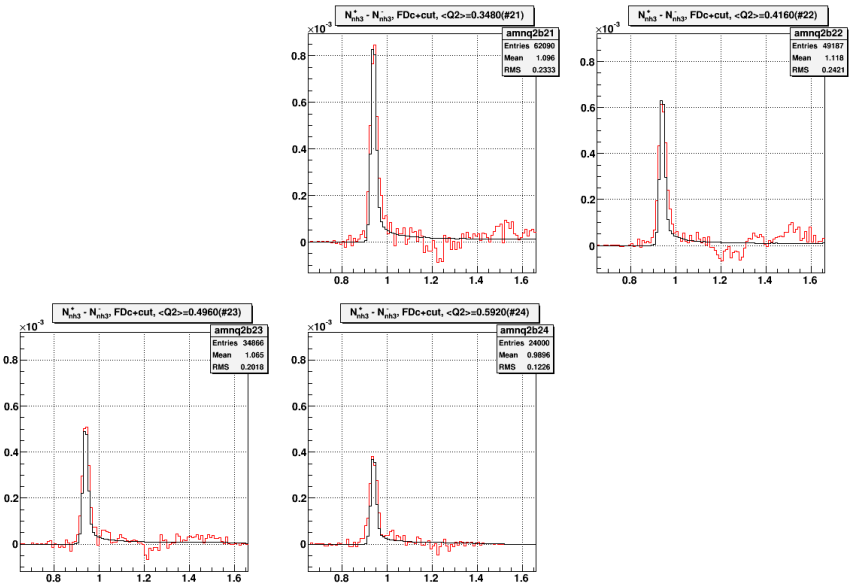

Figure 6: Difference of cross sections vs invariant mass (W) from 3.0GeV data. Red from data and Black from simulation. A small negative peak is not visible between 0.9 and 0.92.

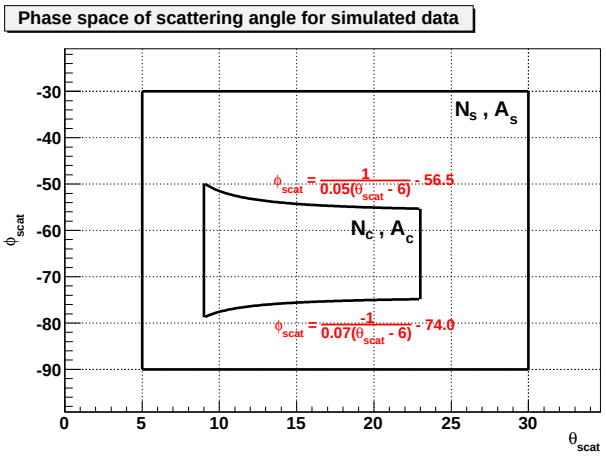

Figure 7: Kinematic coverage of simulations(Rectangle) and the fiducial cuts

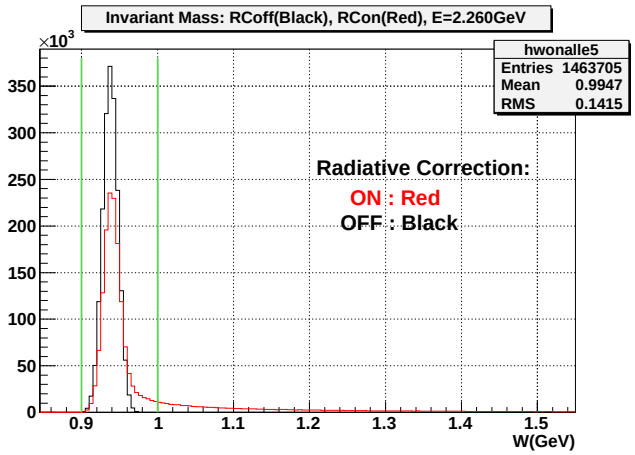

Figure 8: Distribution of invariant mass for elastic e-p scattering difference of cross section from simulated data with radiative effect(Red) and without the effect(Black)

figure 1, is used for selecting the events. Elastic asymmetries and unpolarized cross sections are calculated theoretically for each event. The difference of cross sections can then be calculated by multiplying the asymmetry by the cross section:

$$\sigma_{diff}^{sim} = \sigma_+ - \sigma_- = 2 \cdot \frac{\sigma_+ - \sigma_-}{\sigma_+ + \sigma_-} \cdot \frac{\sigma_+ + \sigma_-}{2} \tag{8}$$

$$= 2 \cdot A \cdot \sigma_{unpol} \tag{9}$$

where A is the elastic asymmetry and σ_{unpol} is unpolarized cross section. To account for bin averaging effects in each θ_{sc} bin, product of elastic asymmetries and cross sections are summed over a bin and normalized to the number of events within the bin. So, eq. 9 for a bin can be written as:

$$\sigma_{diff}^{sim} = 2 \langle A \rangle \frac{1}{N_c} \frac{d\sigma}{d\Omega}|_{bin} \tag{10}$$

$$= 2 \frac{\sum A \frac{d\sigma}{d\Omega}}{\sum \frac{d\sigma}{d\Omega}} \cdot \frac{1}{N_c} \sum_1^{N_c} \frac{d\sigma}{d\Omega} = \frac{2}{N_c} \sum A \frac{d\sigma}{d\Omega} \tag{11}$$

where N_c is the number of events per $\langle \theta_{sc} \rangle$ bin.

3.1 Radiative Effects in simulation

In this simulation, internal and external bremstralhung, multiple scattering and vaccum polarizations are applied. It is assumed that the materials within 10cm from the target are encountered to scatterings. By setting the variable, "ponly" to 1, the simulation forces the reaction from the target material only.

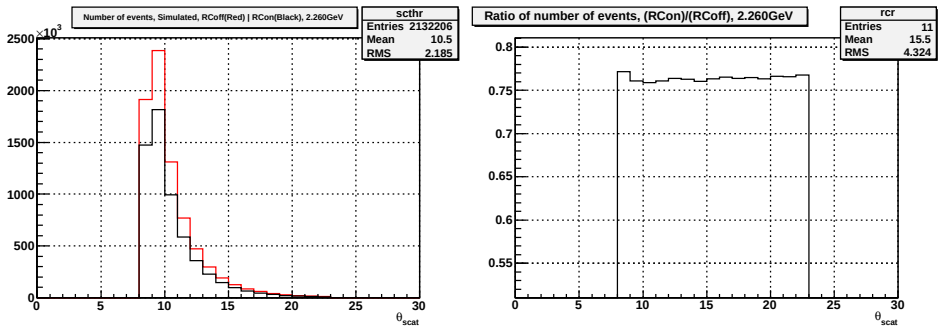

Figure 9: (Left)Distribution of number of counts for study of Radiative effects: With corrections(Black) and without (Red). The right plot shows the ratio of them.

3.1.1 Energy loss

Bremstralhung is applied to simulate the energy loss from a material when an electron passes through.

External Bremstralhung The probability of an electron passing through the material with initial energy E_0 to lose energy ΔE by external bremstralhung is given by

$$P_e(E_0, \Delta E, t) = \frac{bt}{\Gamma(1+bt)} \left(\frac{\Delta E}{E_0}\right)^{bt} \frac{1}{\Delta E} \tag{12}$$

where t is thickness of the material, Z is charge number of the material and Γ is the gamma function. The parameter b is given by:

$$b = \frac{4}{3}\left(1 + \frac{Z+1}{9\left\{ln(1194Z^{-2/3}) + Zln(184.15Z^{-1/3})\right\}}\right) \tag{13}$$

Internal Bremstralhung The probability distribution of energy loss by internal bremstralhung is given by[4]:

$$P_{int}(E_0, \Delta E, \nu) = \frac{\nu}{\Gamma(1+\nu)} \left(\frac{\Delta E}{E_0}\right)^{\nu} \psi\left(\frac{\Delta E}{E_0}\right) \tag{14}$$

where E_0 is the initial energy, ΔE the energy loss and parameter ν is:

$$\nu = \frac{\alpha}{\pi}\left(ln\frac{Q^2}{m_e^2} - 1\right) \tag{15}$$

In the simulation, the energy loss is determined by:

$$\Delta E = E_0 R^{1/bt(\nu)} \tag{16}$$

. And its distribution will look like the distribution of eq. 12 and 14.[10] In each material an electron 's passing through, this energy loss is computed with a half length of the material and multiple scattering is considered with its full length. Then the other half of the length is used to update the energy loss after the multiple scattering.

3.1.2 Multiple Scattering

A charged particle is deflected by many small-angle scatters when it passes through the material. It experiences the Coulomb field of the nuclei. For small deflected angle, the distribution of Coulomb scattering roughly follows the Gaussian distribution but for larger angle it follows Rutherford scattering. For many applications to use a Gaussian approximation, a width given below is sufficient for the central 98% of the angular distribution:

$$\theta_0 = \frac{13.6MeV}{E}\sqrt{R_l}\,[1 + 0.038ln(R_l)] \tag{17}$$

where E is the energy of an incoming particle and R_l is the thickness of material in radiation lengths.

In simulation, eq.17 is multiplied to simulate the scattering angles from a Gaussian distribution:

$$\Delta\theta = \theta_0\sqrt{-2lnR_1}cos(2\pi R_2) \tag{18}$$
$$\Delta\phi = \theta_0\sqrt{-2lnR_1}cos(2\pi R_2) \tag{19}$$

where R_1 and R_2 are random number within [0,1].

3.1.3 Cross section and Target

Simulation code computes the unpolarized electron-proton cross sections via Rosenbluth Formula[11]:

$$\frac{d\sigma}{d\Omega} = \left(\frac{d\sigma}{d\Omega}\right)_{mott}\left\{\frac{{G_E^p}^2 + \tau {G_M^p}^2}{1+\tau} + 2\tau {G_M^p}^2 tan^2\frac{\theta}{2}\right\}. \tag{20}$$

where

$$\frac{d\sigma}{d\Omega}\Big|_{mott} = \frac{\alpha^2}{4E^2 sin^4\frac{\theta}{2}}\frac{E'}{E}cos^2\frac{\theta}{2} \tag{21}$$
$$G_E^p = \frac{1 - 0.13(Q^2 - 0.04)}{(1 + Q^2/0.71)^2} \tag{22}$$
$$G_M^p = \frac{\mu_p}{(1 + Q^2/0.71)^2}. \tag{23}$$

Eq.21 is mott scattering and eq. 22 and 23 are electric(E) and magnetic(M) form factor of proton(p) respectively. $\tau = Q^2/4M$ and μ_p is magnetic moment in unit of nuclear magneton.

Also, Elastic asymmetry is computed to obtain the difference of cross sections[12]:

$$A = \frac{\tau G_M^p}{G_E^p} \frac{\frac{2M}{E} + \frac{G_M^p}{G_E^p}\left[\frac{2\tau M}{E} + 2(1+\tau)tan^2\frac{\theta}{2}\right]}{1+\tau\left(\frac{G_M^p}{G_E^p}\right)^2\left[1+2(1+\tau)tan^2\frac{\theta}{2}\right]}. \tag{24}$$

3.2 Calculation of simulated cross section difference

It is necessary to normalize simulated cross section differences to obtain the σ_{diff}^{sum} per each $\langle\theta_{sc}\rangle$ bin. Summed difference in eq.11 is obtained via simulated cross sections with radiative effects. Due to this effect, the peak in the elastic region, 0.9<W<1.0, gets smaller and developes a tail at larger W values compared to the peak without radiations. Therefore, each $\langle\theta_{sc}\rangle$bin loses its statistics by approximately the amount of an area due to the part of a radiative tail that is cut out. However, that amount is originally within the elastic region if there is no radiative effecs. As far as the "radiated" cross section is concerned, normalization factor N_c in eq.11 will be the number of elastic events without radiative effects per $\langle\theta_{sc}\rangle$ bin. Now, eq. 11 is to be written more explicitly:

$$\sigma_{diff}^{sim} = \frac{2}{N_c^{RCoff}} \sum A \frac{d\sigma}{d\Omega}|_{RCon} \tag{25}$$

And its uncertainty is given by:

$$\frac{\left(\Delta\sigma_{diff}^{sim}\right)^2}{\left(\sigma_{diff}^{sim}\right)^2} = \frac{\left(\Delta N_c^{RCoff}\right)^2}{\left(N_c^{RCoff}\right)^2} \tag{26}$$

$$\Delta\sigma_{diff}^{sim} = \sigma_{diff}^{sim}\frac{\Delta N_c^{RCoff}}{N_c^{RCoff}} = \sigma_{diff}^{sim}\frac{\sqrt{N_s p\,(1-p)}}{N_c^{RCoff}} \tag{27}$$

$$= \sigma_{diff}^{sim}\frac{\sqrt{N_c^{RCoff}\,(1-p)}}{N_c^{RCoff}} \tag{28}$$

where $p = A_c/A_s$ and $N_c^{RCoff} = N_s \cdot A_c/A_s$.

Figure 9 shows distributions of yields with the radiative effect and without the effect. Distribution(Black) is scaled due to the radiative effects. See also figure 10 for difference of cross sections.

4 Ratio of difference of cross sections

The ratio of difference of cross sections is shown on fig. 11. Its error bar is constructed via this equation:

$$\sigma_{diff}^{ratio} = \sigma_{diff}^{exp}/\sigma_{diff}^{sim} \tag{29}$$

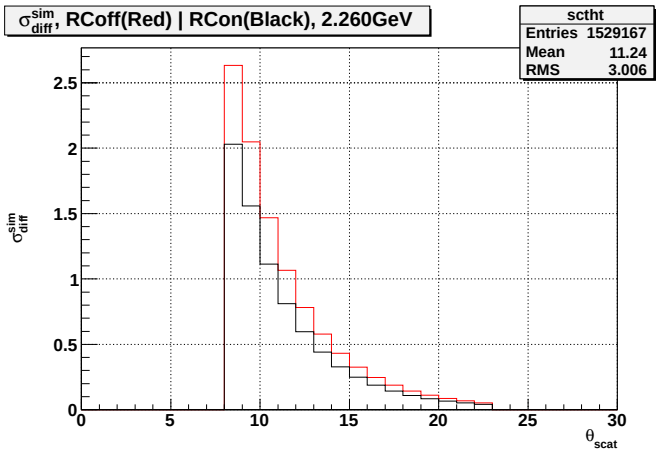

Figure 10: Simulated difference of cross sections for radiative effects on(Black) and off(Red)

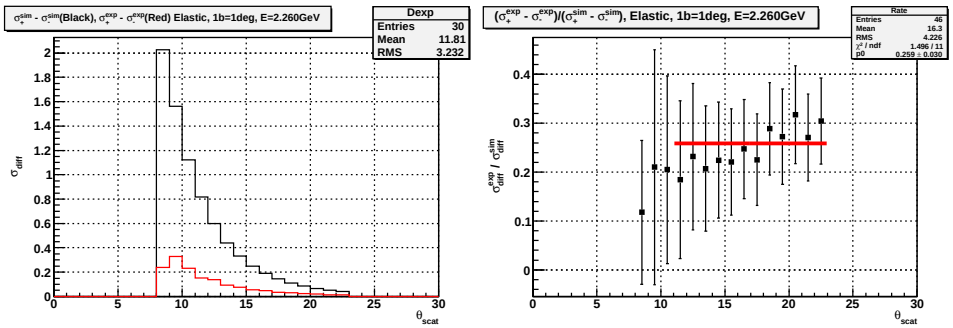

Figure 11: Difference of cross sections from experimental(Red) and simulated(Black) data respectively(left). Ratio of these two (right). The ratio is obtained from fitting with a preliminary value of 0.2589 +/- 0.0303

θ	$\frac{N^+}{fc^+} - \frac{N^-}{fc^-}$	$\sigma^{exp}_{diff}(\mu b)$
11.0 - 12.0	1.39202×10^{-5}	0.1506690
14.0 - 15.0	7.82773×10^{-6}	0.0743568
17.0 - 18.0	3.88847×10^{-6}	0.0323355

Table 1: Results from experimental data for chosen angle bins.

$<\theta>$	$\sigma(\mu b)$	A	$2\cdot A\cdot\sigma$	$RCon/RCoff$	$2A\sigma(on)/(off)$	$\sigma^{sim}_{diff}(\mu b)$
11.5	4.786488	0.110744	1.060153	0.760957	0.806731	0.811216
14.5	1.329269	0.161903	0.430426	0.760540	0.327356	0.328786
17.5	0.431839	0.216603	0.187075	0.764078	0.142940	0.143449

Table 2: Results from calculations by hand and compared with simulated data. The last two columns have to be compared.

$$\left(\Delta\sigma^{ratio}_{diff}\right)^2 = \left(\frac{\sigma^{exp}_{diff}}{\sigma^{sim}_{diff}}\right)^2 \left[{\sigma^{sim}_{diff}}^2{\Delta\sigma^{exp}_{diff}}^2 + {\sigma^{exp}_{diff}}^2{\Delta\sigma^{sim}_{diff}}^2\right] \quad (30)$$

$$\Delta\sigma^{ratio}_{diff} = \sigma^{ratio}_{diff}\sqrt{{\sigma^{sim}_{diff}}^2{\Delta\sigma^{exp}_{diff}}^2 + {\sigma^{exp}_{diff}}^2{\Delta\sigma^{sim}_{diff}}^2} \quad (31)$$

The difference of cross sections obtained from experimental data contains some factors such as product of beam and target polarizations, packing fraction and detector efficiencies. If it is normalized to the simulated results, the ratio gives the products of those factors. More explicitly it is:

$$\sigma^{ratio}_{diff} = \sigma^{exp}_{diff}/\sigma^{sim}_{diff} = P_bP_t\cdot PF\cdot DE \quad (32)$$

where PF and DE are Packing Fraction and Detector Efficiencies respectively. So the fitted results in fig. 11 gives the product of these factors and if detector efficiencies are evaluated, it will give P_bP_t·PF. The numerical results from the experiment(Table 1) and from the simulation(Table 2) are given.

5 Conclusion

Compared with measurements from NMR[8][9], it doesn't look good: In fig. 9, the ratios seem to have a θ dependence. For this, distribution of the ratios is fitted again with linear function in fig. 12 and compared to the results from constant function. The results are:

$$\sigma^{ratio}_{diff} = 0.259(\pm0.030) \quad (33)$$

$$\sigma^{ratio}_{diff} = 0.07769(\pm0.17551) + [0.01005(\pm0.00958)]\,\theta_{scat}. \quad (34)$$

Here, the difference between the fits gives an estimates of a systematic error due to the possible(unphysical) dependence of the ratio with θ scattering. And there are more things to be done:

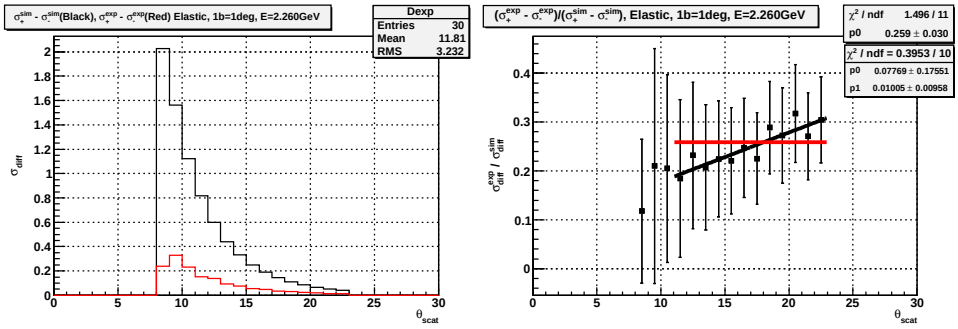

Figure 12: Same as fig. 11. Comparison of two different fit functions. Red line is constant function and its chi-square is 1.496/11. Black line is a linear function and its chi-square is 0.3953/10. Statistical errors are too big.

- polarization of ^{15}N,
- detector efficiencies,
- moving to full GSIM for simulated results.

References

[1] A. Deur , *Private Communications*

[2] S. Stephanyan, *Private Communications*

[3] R. De Vita, *Measurement of the Double Spin Asymmetry in π^+ Electroproduction with CLAS*, PhD thesis, University of Genova, 2000

[4] A. Deur, *Single Arm Monte Carlo for polarized ^{3}He experiments in Hall A.*, Tech note for e94010, LPC/University Blaise Pascal, 2000

[5] S. Phillips, *EG4 wiki, Fcup/BPM Ratio Analysis, July 2,2010*, http://clasweb.jlab.org/rungroups/eg4/wiki/index.php/July_2%2C_2010 , 2010

[6] M. Ripani, *EG4 analysis reference page*, http://www.jlab.org/Hall-B/secure/eg4/ripani/Reference/Reference.html , 2010

[7] M. Osipenko et al, *Matching between the electron candidate track and the Cherenkov counter hit* , CLAS NOTE 2004-020 , 2004

[8] K. Slifer, *EG4 Moller Measurements.*, Tech note # 2, 2006

[9] K. Slifer, *Private Communications*

[10] G. Miller, *Inelastic electron scattering at large angles.*, SLAC Report 129, 1971

[11] A. Thomas, *The structure of the nucleon.*, Wiley-vch, 2001

[12] M. J. Alguard et al, *Elastic Scattering of Polarized Electrons by Polarized Protons.*, Phy. Rev. Lett. **37**, 19, 1976